Research on Engineering Structures & Materials
www.jresm.org
MIM Research Group

Research Article

Development and characterization of plasma electrolytic oxidation coatings on AA5052 for advanced solar reflector thermal control

Ravi Kumar [1,a], Vinod Kumar [1,b], Himanshu Sah [1,c], Nithiyapathi C [2,d], Nischal P Mungle [3,e], P Satishkumar [*,4,f]

[1]*Dept. of Mechanical Engineering, BTKIT Dwarahat, Almora, Uttrakhand, India*
[2]*Dept. of Aeronautical Engineering, Nehru Institute of Engineering and Technology, Coimbatore, Tamilnadu, India*
[3]*Dept. of Mechanical Engineering, Yeshawantrao Chavan college of Engineering, Wanadongari, Nagpur, India*
[4]*Dept. of Mechanical Engineering, Rathinam Technical Campus, Coimbatore, Tamilnadu, India*

Article Info

Article History:

Received 12 Oct 2025
Accepted 20 Apr 2026

Keywords:

Absorbance;
Emittance;
Plasma electrolytic oxidation;
Viscosity;
Time;
Pulse frequency;
Current density;
Sulphuric acid;
Sodium silicate

Abstract

Numerous subsystems make up a spaceship, requiring temperatures within narrow parameters to perform at peak performance. By carefully choosing the thermal and optical characteristics, notably solar absorption and infrared Emittance, the passive thermal controller plays a crucial part in keeping spaceship components within the necessary temperature ranges. Plasma electrolytic oxidation (PEO) of AA5052 studies to develop a solar glass coating suitable for use in outer space. An electrolyte of sodium silicate (Na2SiO3) to create these coatings. Specifically, the layer's thermal and optical performance is investigated as a function of pulse on time, process time and pulse frequencies, and the electrolyte composition used. The PEO coating thickness is personalized to achieve thermo-optical qualities on par with or better than those achieved with standard sulphuric acid anodizing. The improved coating is put through its paces to ensure it can function as a thermal control surface in space, with testing including adhesion, humidity, and performance in simulated space conditions including thermal cycling and thermo-vacuum. The morphological, microstructural characteristics, and arrangement of coatings achieved through the PEO progression and conventional sulphuric acid anodizing are compared using X-ray diffraction (XRD), scanning electron microscopy (SEM), and energy dispersive X-ray spectroscopy (XPS).

1. Introduction

The One side of a spaceship may be subjected to intense heat from the sun, while the other is subjected to freezing conditions in interplanetary space [1]. Even more so, as the spacecraft enters an eclipse, some of its non-operational components endure shallow temperatures while its operational features experience higher temperatures [2]. This severe thermal environment imposes a temperature difference of several hundred degrees Celsius. However, there is a small temperature range in which the various spacecraft components and electronics can operate at their optimum [3]. Thermal control is a fundamental design consideration to keep all mission subsystems within their temperature limits throughout the task. Using surfaces with suitable

*Corresponding author: sp.sathishkumar10@gmail.com
[a]orcid.org/0000-0001-7778-6126; [b]orcid.org/0009-0005-8747-718x; [c]orcid.org/0009-0006-9643-2538; [d]orcid.org/0000-0002-7461-7738; [e]orcid.org/0000-0003-4627-5811; [f]orcid.org/0000-0002-0574-3482
DOI: http://dx.doi.org/10.17515/resm2026-1244ma1012rs

thermo-optical properties, like absorption (α)and Emittance (Ɛ), passive thermal control methods provide very reliable temperature management of spaceship components [4-6].

Aluminum undergoes anodization, also known as electrochemical oxidation when it is immersed in an electrolyte solution and then electrolyzed to create a thin, protective oxide layer on its surface [7]. Emittance values as low as 0.03 can be achieved on a polished aluminum metal surface; this value can be significantly improved with anodization. The IR emissivity of a conventionally anodized sulfuric acid coating is 0.77, but the solar absorption is only about 0.34 [8,9]. As a result, the anodic film acts as a highly effective solar reflector. However, there are environmental concerns with the anodization process due to the use of powerful acids and the difficulty in properly disposing of them [10-12]. As a result, there is perpetual pressure to find a better coating method that may enhance functional characteristics while still satisfying the demanding standards of current environmental regulations [13].

The basic idea is the same as anodizing, but the voltages are much higher, and the oxide is formed through a dielectric breakdown in the form of micro-discharges [14,15]. Generally speaking, researchers agree that all variations of the PEO process can be deemed environmentally friendly, as the electrolyte employed for this process comprises mild alkaline solutions [16-18]. Coatings made from polyethylene oxide (PEO) are renowned for protecting against corrosion, increasing hardness, and resisting heat and electricity. In recent literature, PEO coatings have even been proposed as an impregnate for sol-gel coating on Al and Mg alloys [19]. PEO coatings have several potential uses, including in the extreme space conditions, but little research has been done on their thermo-optical properties [20]. This study aims to use plasma electrolytic oxidation to create an oxide layer on AA 5052 alloy for heat management applications. Authors systematically examine the impact of various operating conditions to achieve an oxide coating with thermo-optical properties similar to those achieved through traditional sulphuric acid anodization.

Due to the inaccessibility of a spacecraft once it has entered orbit and the extreme corrosiveness of space settings, coatings developed for usage in space applications require higher standards and more excellent dependability [21]. Coatings like this need to endure the extreme heat and pressure of the launch phase, the vacuum of space, ionizing radiation, high-energy charged particles like electrons and protons, and wildly fluctuating temperatures in orbit [22], [23]. If coatings on spacecraft parts aren't applied perfectly, it could negatively affect the functionality of a certain subsystem, which could cause problems throughout the spacecraft. Therefore, the coatings obtained using the finalized parameters are put through a battery of tests to determine whether or not they are suitable for use in space, including adhesion and humidity testing, thermal cycling, and thermo-vacuum experimental tests [24]. These expedited tests disclose any change in the coating's s and IR values that may have occurred over the spacecraft's entire operational lifetime [25], [26]. SEM, EDX, XPS, and XRD are all used to learn more about the coating.

Friction riveting is an emerging technique for joining lightweight materials; however, its application is limited by the requirement of specialized force-controlled equipment. [27]. This study focuses on the development of Al-based metal matrix nanocomposites reinforced with graphene nanoplatelets (GNP) using powder metallurgy. The results show that the addition of GNP significantly enhances mechanical properties and corrosion resistance compared to pure aluminum [28]. Metal matrix composites (MMCs) exhibit superior mechanical and tribological properties compared to base alloys. [29]. The water-quenched Cr-reinforced Al/Cu composites exhibit superior hardness, compressive strength, and wear resistance compared to oil-quenched samples [30.

Although plasma electrolytic oxidation (PEO) coatings have been widely investigated for thermal control applications on aluminum alloys, limited studies have systematically addressed the behavior of Mg-containing AA5052 and the influence of electrolyte concentration on its thermo-optical performance and long-term environmental stability. A systematic correlation between Na_2SiO_3 electrolyte concentration, discharge characteristics, coating morphology, and resulting solar absorptance (α) and infrared emittance (ε) is established. Furthermore, unlike earlier studies, the optimized coatings are subjected to comprehensive space-simulated environmental testing, including thermo-vacuum, thermal cycling, and humidity exposure. This combined approach

provides both process-level optimization and application-level validation, contributing to the development of durable and environmentally sustainable thermal control coatings for spacecraft applications.

2. Experimental Procedure

Samples of AA5052 alloy in the form of disks are developed using plasma electrolytic oxidation coating using a silicate-based electrolyte. The plasma electrolytic oxidation (PEO) treatment was carried out using a pulsed DC power supply under galvanostatic mode at an applied current density of 10 $A \cdot dm^{-2}$, with a corresponding voltage range of 300–520 V during the oxidation process. A pulse frequency of 1000 Hz and a duty cycle of 20% (ton/toff controlled) were maintained throughout the treatment. The total processing duration was 15 minutes for all coated samples. The electrolyte consisted of an aqueous sodium silicate (Na_2SiO_3) solution at optimized concentration of 90 gl-1, and the temperature was maintained below 30°C using continuous stirring and external cooling to ensure stable discharge behavior and uniform coating growth. The samples are degreased in room-temperature isopropyl alcohol for 10 minutes to get rid of any oil, lubricant, or dust. Rinsing the specimen with distilled water follows. A polypropylene tank with a 25 ltr capacity holds the electrolyte, a sodium silicate solution with a concentration of $30gl^{-1}$. Authors used the sample as the anode and a thin sheet of stainless steel for the cathode. For this procedure, we employ a 25kW custom-built PEO power supply. This procedure utilizes a positive, unipolar, square-wave pulsed current. The processing tank has stainless steel cooling coils installed inside, which circulate cold water to maintain an electrolyte temperature below 25°C. The cleaned and prepped samples are given a final rinsing in DM water before being dried with a hot air pistol.

Several factors, including pulse frequency, electrolyte arrangement, mean current density, process time, and pulse on time, are studied to understand the coating's thermo-optical performance better [31]. The concentration of Na_2SiO_3 is varied from 30 gl^{-1} to 150 gl^{-1}, and the average current density is held constant at 9 Adm^2 for 35 minutes. With a steady pulse frequency of 400 Hz and pulse on-time of 550 µs, a duty cycle of 15% is achieved. To examine the effect of process time on coating viscosity and the associated thermal and optical characteristics, samples are processed at a mean current density of 9 A dm^2 for 15, 25, 35, 45, 55, and 65 minutes employing a 90 gl^{-1} Na_2SiO_3 electrolyte. To analyze the impact of pulse frequency on the thermal and optical characteristics, specimens are generated at variant frequencies (100, 250, 400, 550, and 700 Hz) while maintaining a constant pulse on-time of 550 µs and a persistent mean current density of 9 Adm^2. Coatings are made with different average current densities (3, 6, 9, 12, and 15 A dm^2) and pulse on time (100, 250, 550, and 700µs) to further examine the impact on thermo-optical properties. On the other hand, traditional anodization calls for a sulphuric acid electrolyte, a current density of $3Adm^2$, and a hydrothermal sealing process of 1 hour in boiling water. To investigate the impact of coating viscosity on thermal, and optical characteristics, specimens are anodized for varying durations (from 15 minutes to 65 minutes).

To process PEO samples of varying thicknesses, a solution containing 90 gl^{-1} Na_2SiO_3 is used, with a mean current density of 9 A dm^2 two and pulse frequencies and pulse on-time, respectively, 400 Hz and 550 µs. The samples are then hydrothermally sealed in boiling water for 1 hour. Next, stuffed specimens are compared to unsealed samples of the same thickness and with the exact specifications regarding their thermo-optical properties.

Each process's voltage-time response is measured and then compared. Each sample was assessed for its coating thickness on both sides, and then statistical procedures were applied to generate an average value with slight variation. The Solar Spectrum Reflectometer (SSR) and the micrometer (AE) are used to measure the absorption and emission [32]. Surface roughness measurements were performed using a Surtronic 3+ stylus profilometer with a cutoff length of 2.5 mm and an evaluation length of 8 mm. For each sample, measurements were taken at six different locations to ensure repeatability, and the average values of Ra (arithmetic mean roughness) and Rq (root mean square roughness) were reported along with standard deviations. The stylus tip radius was 5 µm, and the applied force was maintained constant to avoid surface damage. Similarly, the Surtronic 3+ is used

to assess the coating's surface roughness utilizing a stylus probe at an evaluation length of 8.00 mm [33,34]. Later, the surface roughness measurements from both techniques are compared.

The energy-dispersive X-ray spectroscopy instrument is permanently attached to the scanning electron microscope and is used to determine the elemental composition of the deposit [35]. For our X-ray diffraction studies, authors employ a Philips X'pert-Pro instrument set to 45 kV and 35 mA, radiating with Cu K rays (α= 1.6206) and scanning from 10° to 100° at a rate of 0.15° s 1 with a step size of 0.03°. A SPECS spectrometer using AlK radiation (1512.6 eV) at 160 W (13 kV, 14 mA) is used to conduct X-ray photoelectron spectroscopy (XPS) experiments on anodized and PEO coatings. The C1 s peak is positioned at 291.7 eV, and binding energies are provided about this value. One uses a pass energy of 80 eV and a step increment of 0.6 eV to acquire the survey spectra, whereas one uses pass energy of 45 eV and a step increment of 0.06 eV to obtain the individual spectra. The Si2p core-level spectra are cleaned of Shirley noise, and then the data is fitted using the Casa XPS program.

The space routineness of a Plasma Electrolytic Oxidation coating is determined by putting it through tests in a space environment simulator after the parameters have been finalized [36]–[38]. The results can be trusted because they are replicated using the same four samples for each test. Coatings are monitored for consistent thermo-optical behavior by measuring their solar absorption (α_S) and infrared Emittance (ε_{IR}) after each environmental test.

3. Results and discussions

3.1 Traditional Anodization Using an Electrolyte of Sulphuric Acid (H_2SO_4)

The influence of processing time on anodic coating thickness is presented in Figure 1. The graphic makes it very clear that the slope of the thickness Vs. after 35 minutes of process time. To rephrase, the coating growth rate slowed after the initial 35 minutes of processing time elapsed. Since the electrical resistance of the coating increases with coating thickness, current flow is delayed, and the coating's growth rate decreases. As the coating thickness increases, the electrical resistance across the oxide layer rises, leading to localized temperature elevation at the metal–electrolyte interface, which reduces the effective coating growth rate due to enhanced oxide restructuring and partial breakdown. The rate of anodic coating breakdown increases with time, causing a decrease in the coating growth rate [39].

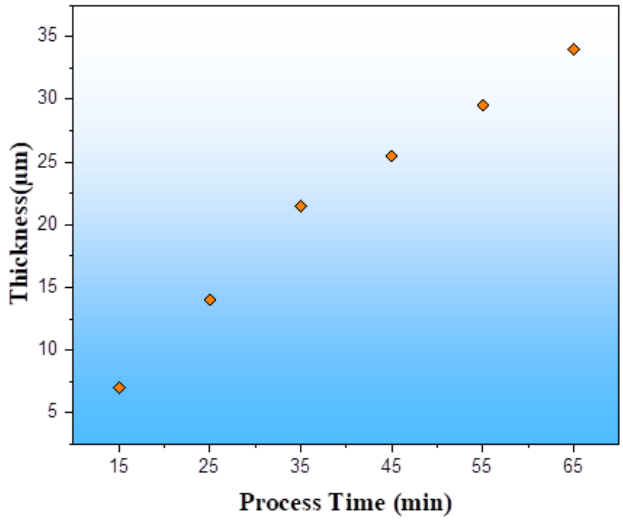

Processing Time (min)	Thickness (µm)
15	7 ± 0.14 µm
25	14 ± 0.28 µm
35	21.5 ± 0.43 µm
45	25.5 ± 0.51 µm
55	29.5 ± 0.59 µm
65	34 ± 0.68 µm

Fig. 1. Comparison of coating thickness and process time for conventional H_2SO_4 anodization

In Fig. 2, authors can see the measurements results of the thermo-optical properties of coatings of varying thicknesses. Coating emittance increased from 0.82 at 7 µm to 0.94 at 21 µm, and further to 0.96 at 35 µm, indicating a significant overall improvement of approximately 17%; however, the rate of increase beyond 21 µm is relatively small, suggesting a saturation trend in emittance with increasing coating thickness. The absorbance of the anodic film increased from 0.342 for a 7µm

coating to 0.378 for a 21µm coating and 0.436 for a 35µm coating. The outcome was a decrease in the α/Ɛ ratio, reaching a minimum at a coating thickness of 25 nm, followed by an increase in that value. The hydrothermally sealed, 42 µm thick anodic coating's 0.382 absorptions and 0.98 emittances make it an effective solar reflector.

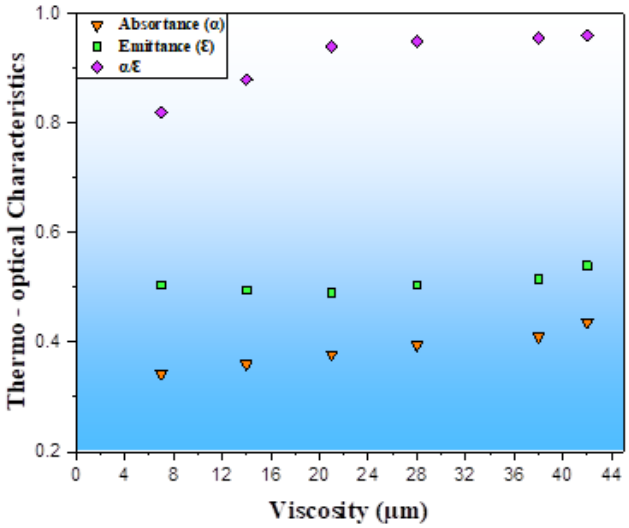

Fig. 2. Thermal optical characteristics of anodic coating on variant viscosity

3.2 Optimum of Plasma Electrolytic Oxidation Processing Factors

3.2.1 Impact of Na_2SiO_3 Concentration

The voltage and process time response are shown to be affected by the sodium silicate content of the electrolyte (Figure 3a). An increase in Na_2SiO_3 in the electrolyte has been shown to drastically reduce the breakdown voltage from 492 V to 324 V. According to prior research by author [40], this behavior can be understood as the result of an increase in the conductivity of the solution with a rise in Na_2SiO_3 of the electrolyte. When the Na_2SiO_3 concentration is 120 gl-1 or higher, the voltage-process time plot also shows significant voltage variations. 1. The metal-oxide boundary is thought to be the source of the powerful and long-lasting sparks responsible for this phenomenon [41,42]. These discharges are considered to the coating growth rate because they prevent the production of a protective oxide layer. Intense fluctuations in voltage as a function of time may be due to the dissolution of an oxide layer that grows thinner with increasing sodium silicate concentration. So, taking everything into account, the best silicate concentration for future studies is 90gl.

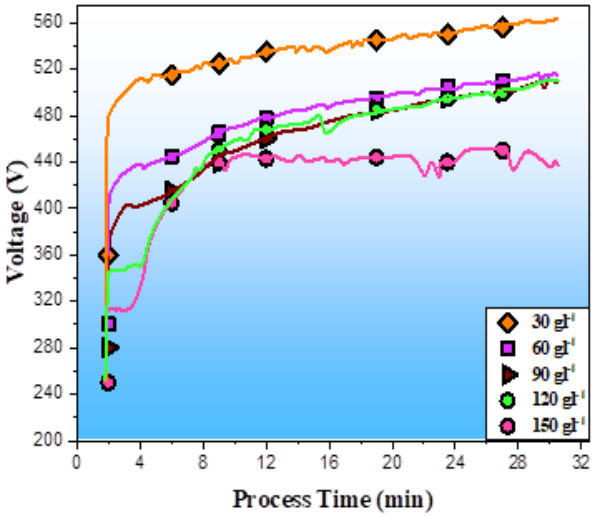

(a)

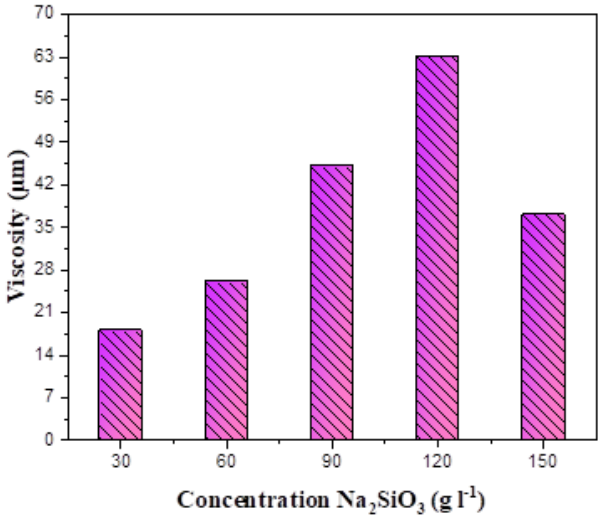

(b)

Concentration Na_2SiO_3 (g l^{-1})	Viscosity (µm)
30	18 ± 0.36
60	26 ± 0.52
90	45 ± 0.90
120	63 ± 1.26
150	37 ± 0.74

Fig. 3. (a) Impact of Na_2SiO_3 on coating viscosity, (b) Impact of Na_2SiO_3 on voltage–process time response

3.2.2 Impact of Process Time

In Fig 4, shows the coating thickness changed as a function of the applied voltage and processing time. Figure 4 illustrates (a) the variation of coating thickness with processing time and (b) the corresponding voltage–time response during the PEO process. When equated to the anodic process, the coating growth rate in PEO is dramatically faster. When correlated to the PEO procedure, which yields a coating thickness of 91 µm after 65 minutes of processing, conventional anodization causes a coating thickness of 35µm. The mechanism for coating production is different, which is the primary factor. Oxide production in the PEO process happens through melting and re-solidifying the previously created oxide layer [43]. Hence the resistances of the oxide layer do not affect the growth rate in any way, in contrast to the anodization process.

The thermo-optical properties are plotted against coating viscosity to determine the thinnest Plasma Electrolytic Oxidation coating that displays qualities identical to anode coating (Fig. 5). Coating emittance improved from 0.81 for a 14µm coating to 0.98 for a 91µm coating. It was determined that an emittance value of 0.98 corresponds to a coating thickness of roughly 42µm, which is on par with a conventionally anodic specimen with a viscosity of approximately 21µm [44]. But the ratio of Absorptance to Emittance systematically decreases as coating thickness grows, going from 0.439 for a 14µm coating to 0.353 for a 91µm coating.

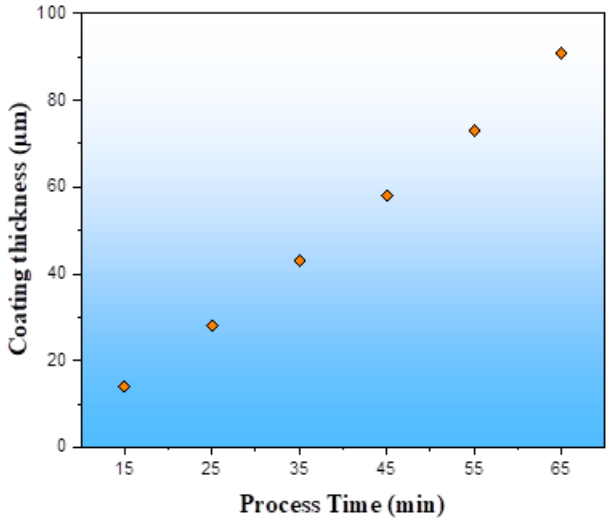

(a)

Process Time (min)	Coating thickness (µm)
15	14 ± 0.28
25	28 ± 0.56
35	43 ± 0.86
45	58 ± 1.16
55	73 ± 1.46
65	91 ± 1.82

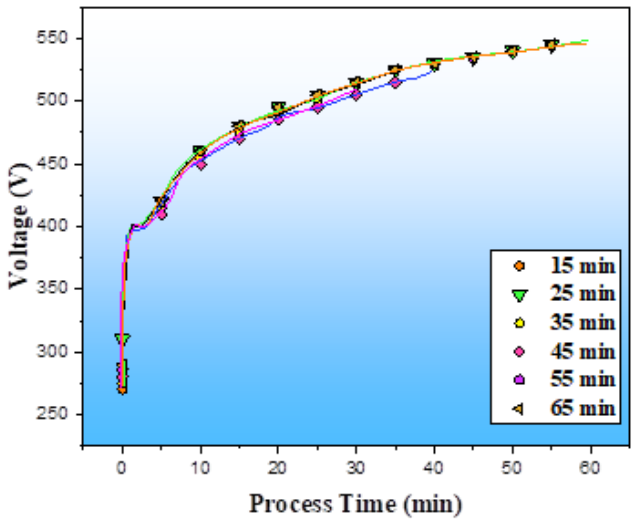

(b)

Fig. 4. (a) Coating thickness Vs. Process time for the specimen in 90 gl^{-1} of Na_2SiO_3 b) Impact of process time on the voltage concerning sample time in 90 gl^{-1} of Na_2SiO_3

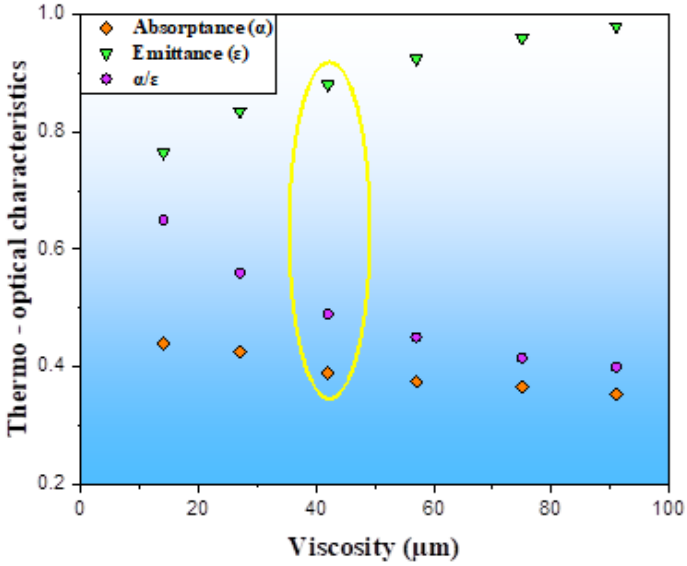

Fig. 5. Thermal optical characteristics concerning coating viscosity

One possible explanation is that various coatings undergo distinct microstructures and compositions due to variations in the underlying process mechanisms [45]. Compared to a typical anodized sample with a 21µm, the absorptance value with a PEO coating thickness of 42µm is 0.382. Therefore, PEO covering 42µm thick was deemed adequate for a solar reflector. This means that 35minutes is the settled-upon process time for the PEO procedure.

3.2.3 Impact of Pulse Frequency

The voltage and process time plot and the resulting coating thicknesses at various pulse frequencies are shown in Figures 6a and b, respectively. When processing at a low frequency of 100Hz, the output voltage rises to a peak of 674.6V after 35 minutes of processing, which is significantly higher than the initial voltage of 571.4 V measured after 1 minute of processing. Since the power source can only produce up to 700 V, working at lower frequencies presents practical challenges, especially with more extensive surface area samples. Furthermore, the low-frequency voltage-time graph demonstrates several voltage changes during the process, albeit of less amplitude. The starting and ending voltages drop dramatically as the frequency rises; at 400Hz, the values are 396.4 V and 510.7 V, respectively. Voltage-time graphs show that significant voltage fluctuations begin at pulse frequencies above 400Hz. This method is found to work best with a pulse frequency of 400Hz. From 100 to 550Hz, there is a slight shift in coating thickness from 33 to

43 µm, and from 550 to 700Hz, the viscosity drops to 42µm (Fig. 6b). Thermo-optical characteristics also change slightly in figure. 6c.

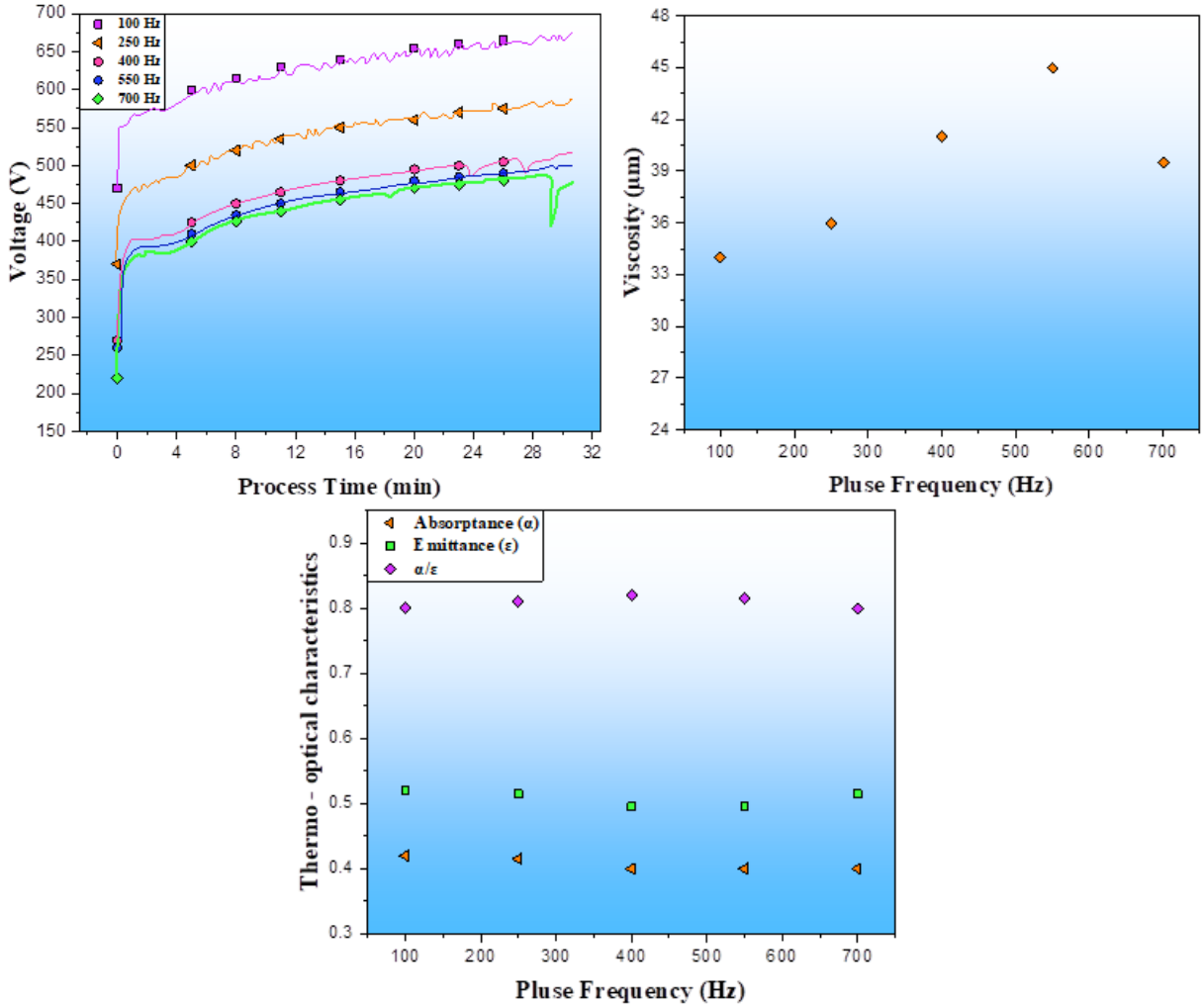

Fig. 6. (a) Impact of process time and voltage concerning pulse frequency, (b) Impact of pulse frequency on the viscosity of coating, and (c)Difference of thermal and optical characteristics function of pulse frequencies

3.2.4 Impact of Pulse On-Time

The rate of growth in the process or the coating does not appear to affect the proportion of on-time occurrences. Sodium silicate's voltage-time response is positively affected by the on-time at a pulse frequency of 400Hz and a mean current density of 9 Adm^2, as illustrated in Figure 7. Coatings developed had a thickness of around 42 m (±3 m). Therefore, their thermo-optical characteristics were also stable. For 35 minutes in a $90gl^{-1}$ electrolyte.

3.2.5 Impact of Mean Current Density

At sufficiently high output voltages, the same pattern emerges in the voltage-time responses over a range of average current densities. It was found that the average current density was approximately linearly related to the coating growth rate and, by extension, the coating thickness. Modifications in thermo-optical characteristics reflect these tendencies. Variation in findings cannot be attributed to average current density alone due to the influence of thermo-optical characteristics on coating thickness. Samples are manufactured at various current densities over varying times to ensure that the average coating thickness is approximately 42 m (±3 m) in each case, removing viscosity's effect on the established impact of average current density on the thermo-optical properties. Assuming a linear rise in thickness with time, the processing time is determined for each average current density by dividing the rate of thickness buildup by the average current density. Accordingly, procedures utilizing average current densities of 3, 6, 9, 12,

and 15 Adm^{-2} call for 100, 48, 34, 22, and 16 minutes, respectively. Fig. 8 shows that the mean current density has little impact on the coating's thermal optical characteristic, as absorption and emittance values are identical for all the layers.

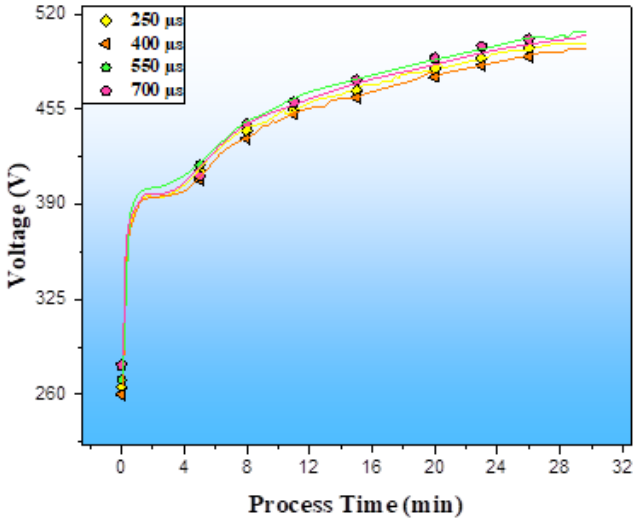

Fig. 7. Impact of process time and voltage concerning pulse on time

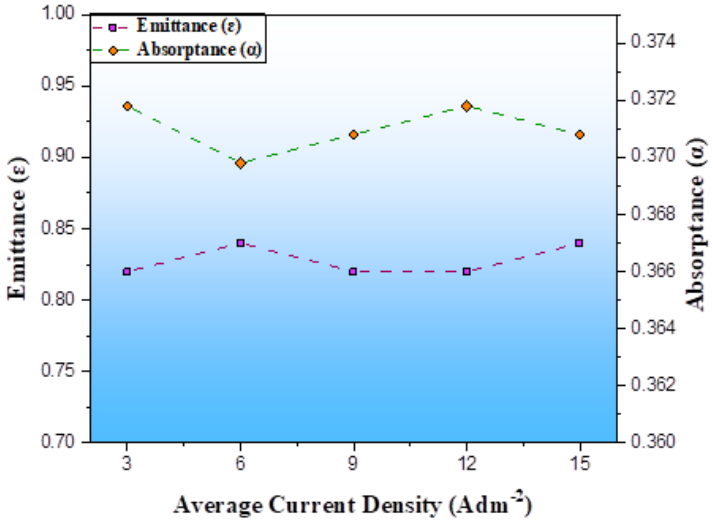

Fig. 8. Thermal optical characteristics of mean current density for Plasma Electrolytic Oxidation coatings of around 42 ± 3µm viscosity

3.2.6 Impact of Hydrothermal Sealing

Thermo-optical characteristics of thin samples were shown to be unaffected by hydrothermal sealing, while thicker models were affected (Fig. 9). It's important to note that the ratio α/Ɛ did not alter even when both emittance and absorption levels decreased. Due to its significance in thermal control design, the α/Ɛ value is shown to be unaffected by hydrothermal sealing without compromising the coating's thermo-optical behavior.

Table 1. Output factors for plasma electrolytic oxidation coating

Electrolyte elements	
Sodium meta silicate ($Na_2SiO_3.9H_2O$)	90 gl^{-1}
Process factors	
Duty cycle	15%
Mean current density	9Adm^{-2}
Pulse on-time	550µs
Processing time	35 min
Pulse frequency	400 Hz

Authors comprehensively study how various operational parameters affect the coating development rate and the coating's thermo-optical behavior to produce a Plasma Electrolytic oxidation coating with a mean viscosity of 42±3 µm demonstrating thermal-optical attributes similar to that of standard anodized coatings. Table 1 displays the fine-tuned processing factors for creating a Plasma Electrolytic oxidation coating with Ɛ=0.81 and α=0.386, ideal for use as a solar reflector.

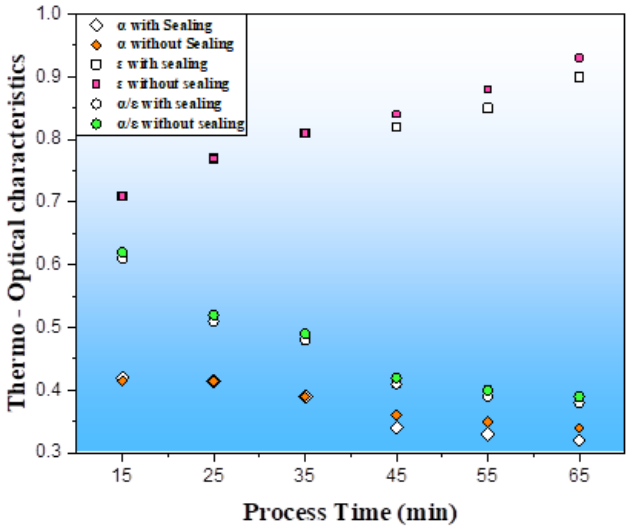

Fig. 9. Hydrothermal sealing of coating after Plasma Electrolytic Oxidation process and its effect on thermal and optical characteristics

3.3 Properties of the Optimum Plasma Electrolytic Oxidation Coating

3.3.1 Coating Existence and Roughness of The Surface

Plasma Electrolytic Oxidation coatings are discovered to be roughly and whitish-grey, in contrast to the anodic coating's smooth and translucent look. Compared to an anodized sample with an RMS roughness of 0.31µm, a PEO-coated model has a roughness of 4.46µm.

Table 2. Surface roughness factors of the anodic specimen and Plasma Electrolytic Oxidation - coated specimen

Roughness factors	Anodized aluminum	PEO coated aluminum
Rq	0.26±0.02 µm	4.34±0.15 µm
Rq	232±5 nm	4528±90 nm
Ra	181±4 nm	3612±72 nm

Table 2 displays the roughness parameters—Rq is the root-mean-square roughness, and Ra (arithmetical mean roughness) is defined as the arithmetic average of the absolute values of the surface height deviations measured from the mean line over the evaluation length, in accordance with ISO 4287—attained for the two coating types. Results are similar to those obtained with a standard contact surface profiler in roughness. In Table 2, first Rq denotes surface profiler and second Rq denotes nano profilometry.

3.3.2 Surface Morphological Properties and Elemental Arrangement

Figure. 10a and b show corresponding scanning electron micrographs of a Plasma Electrolytic Oxidation -coated specimen and an anodized specimen. On the other hand, PEO-coated characters showed a very distinct morphology under the same magnification, most likely because of the differing coating growth mechanism involved in the two processes. Comparatively bigger pores can be seen in the Plasma Electrolytic Oxidation coated specimen compared to the anodized sample.

Immersing the anodized specimen in demineralized (DM) water at or near boiling temperature generates minor fractures in the film's surface, known as hot water sealing. Due to the enormous difference in the coefficient of thermal expansion between metallic aluminum and aluminum oxide, thermal pressures can cause anodic coatings on aluminum to crack or craze. The method of coating growth inherent to PEO coating is responsible for its characteristic shape. When the breakdown voltage is reached, the coating dielectrically breaks down, forming several discharge channels. The coating material melts due to the high temperature produced by the micro-discharges, and the liquid is then ejected down the discharge channels. As the electrolyte cools the molten material, the structure takes on a volcanic aspect as the gaseous products escape through the discharge channels. The increasing oxide layer undergoes multiple cycles of melting, melt flow, re-solidification, and sintering, which results in a consistent and uniform increase in coating thickness. Moreover, microcracks appear on the coating due to the inherent tension caused by the deposition process.

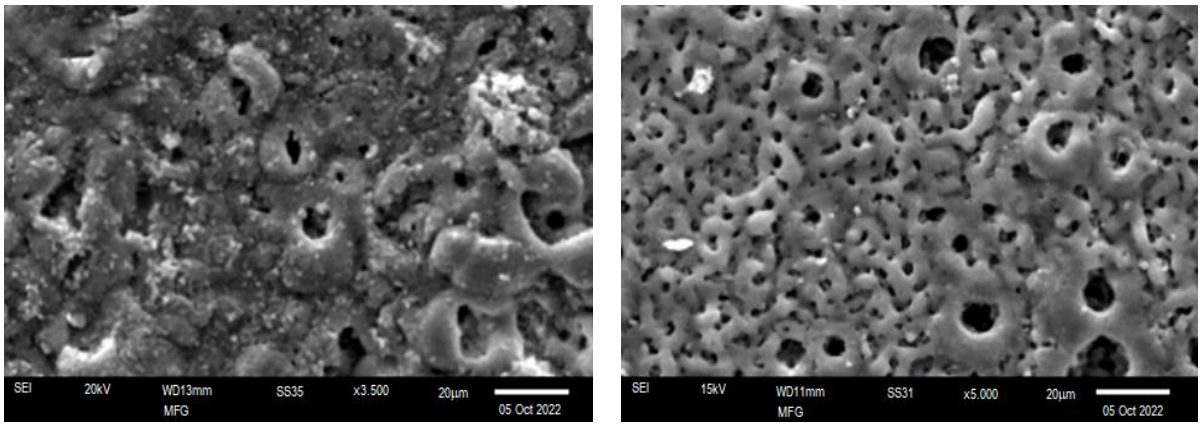

Fig. 10. Scanning electron microscopic images of (a) plasma electrolytic oxidation -coated specimen and (b) anodic specimen

Immersing the anodized specimen in demineralized (DM) water at or near boiling temperature generates minor fractures in the film's surface, known as hot water sealing. Due to the enormous difference in the coefficient of thermal expansion between metallic aluminum and aluminum oxide, thermal pressures can cause anodic coatings on aluminum to crack or craze. The method of coating growth inherent to PEO coating is responsible for its characteristic shape. When the breakdown voltage is reached, the coating dielectrically breaks down, forming several discharge channels. The coating material melts due to the high temperature produced by the micro-discharges, and the liquid is then ejected down the discharge channels. As the electrolyte cools the molten material, the structure takes on a volcanic aspect as the gaseous products escape through the discharge channels. The increasing oxide layer undergoes multiple cycles of melting, melt flow, re-solidification, and sintering, which results in a consistent and uniform increase in coating thickness. Moreover, microcracks appear on the coating due to the inherent tension caused by the deposition process.

The EDX spectra of the PEO coating and the anodic coating (Figure 11b) are presented. Insets depict the parts of each coating type. There is little sodium in PEO coatings, along with Al, SiO2, and O2 (Fig. 11a). Anion species from the electrolyte, most notably SiO32, contribute to the development of the coating, accounting for its comparatively high silicon content. Anionic species in the electrolyte enter the channel via electrophoresis under the influence of the strong electric field during the ejection of molten materials through the discharge channels, react with the molten material, and become incorporated into the coating during the rapid solidification process. The incorporation of the cationic species of the electrolyte into the layer during the plasma discharges is responsible, to a lesser extent, for the presence of sodium in the coating. The anodic coating consists mainly of aluminum and oxygen, with smaller amounts of sulfur (3.14 atomic %) and silicon (trace amounts) (Fig. 14b). Anodizing in a sulphuric acid electrolyte incorporates SO42 ions into the anodic oxide layer, giving the film a sulfurous tint. Because silicon is an alloying element in AA 5052, trace amounts of silicon can also be found in the coating.

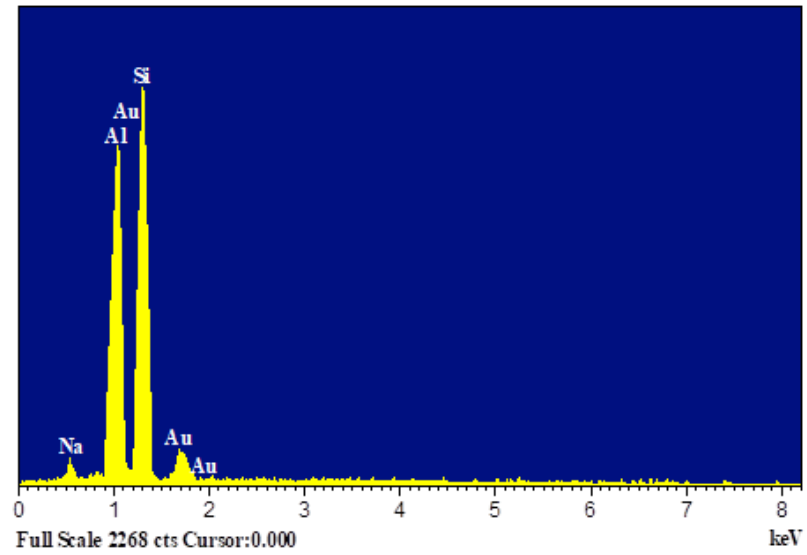

(a)

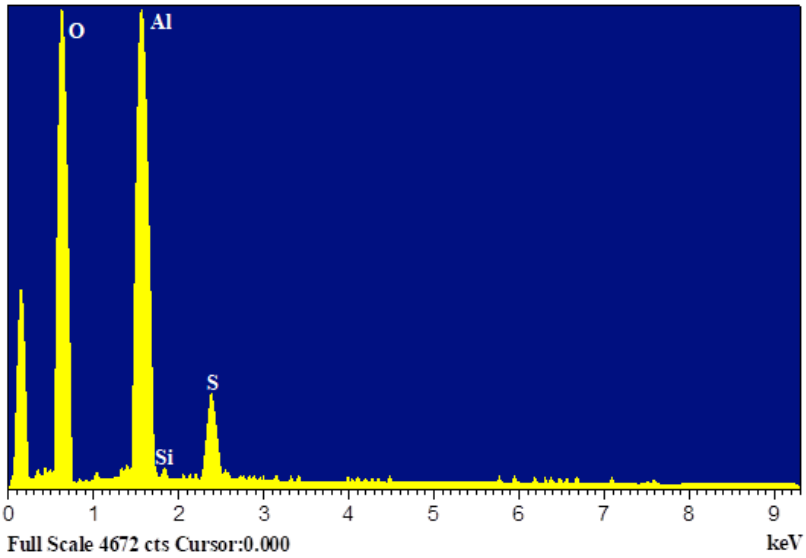

(b)

Fig. 11 Energy Dispersive X-ray spectroscopy and elemental analysis of (a) plasma electrolytic oxidation -coated specimen and (b) anodized specimen

3.3.3 X-Ray Diffraction Analysis

The X-ray diffraction patterns for PEO and anodic coatings are displayed in Figures 12a and b, respectively. Aluminum (substrate) peaks at two values of 41.5°, 47.2°, 69.2°, 81.2°, and 85.8° were attributed in the XRD examination of both coatings.

When X-ray diffraction (XRD) patterns are examined, they show that neither the PEO nor the anodic coatings have any microstructure discernible to the X-ray beam. Peaks in the XRD pattern consistent with aluminum may be traced back to the aluminum in the substrate thanks to the way X-rays can pass through the coating and into the substrate.

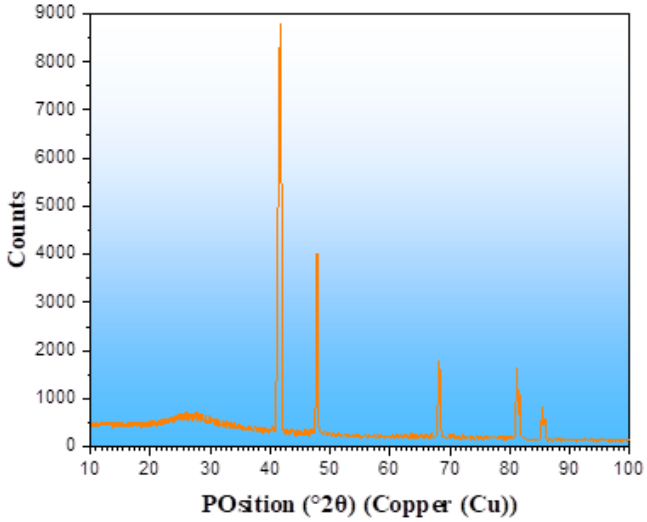

(a)

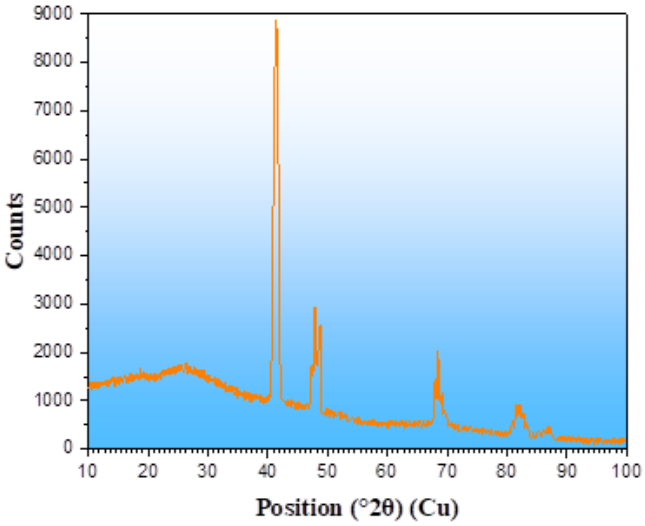

(b)

Fig. 12. XRD pattern of (a) plasma electrolytic oxidation -coated specimen and (b) anodic specimen

3.3.4 Analysis of X-Ray Photoelectron Spectroscopy

XPS survey spectrum of anodic and Plasma Electrolytic Oxidation coatings are displayed in Figure 13. Al and O species can be seen in the ranges of an anodized coating, while Si and O can be seen in a PEO coating's spectrum. Figure 14a displays the XPS data for the Aluminum core levels of the anodic and Plasma Electrolytic Oxidation layers. Al2p has a peak at 75.3 eV in the anodized coating, and this energy is attributed to Al2O3. However, PEO coating has a modest Al2p elevation. Coatings made of polyethylene oxide (PEO) have a broad Si2p core-level spectrum, representing the existence of several Silicon species.

Presented in Fig. 14b is a curve fit into the component-peak form of this spectrum. Peaks in the Si2p range at 104.6, 107.8, and 109.8 eV represent SiO, alumino-silicate, and Si-OH species. These peaks are 24, 65, and 18% concentrated, respectively. To be clear that the alumino-silicate species predominate in this region. Spectra at the oxygen score level for both coatings are depicted in Figure. 14c. The oxide of alumina/alumino-silicate species accounts for the dominant peak at 534.2 eV.

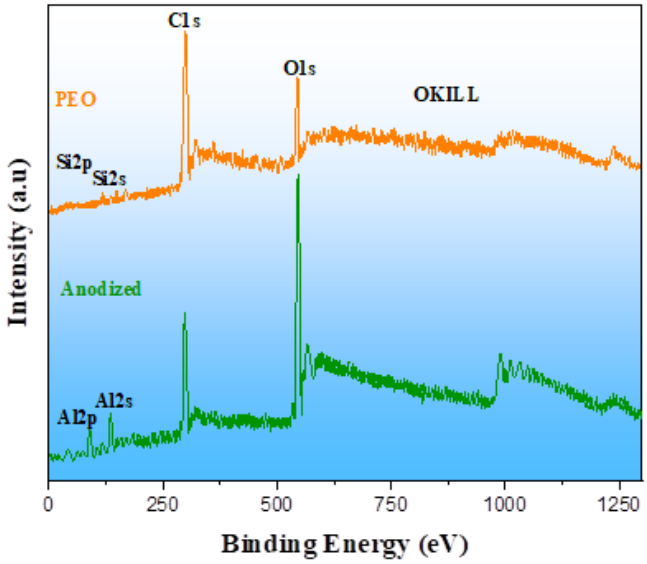

Fig. 13. Survey spectrum of anodic and Polyethylene Electrolytic Oxidation coatings

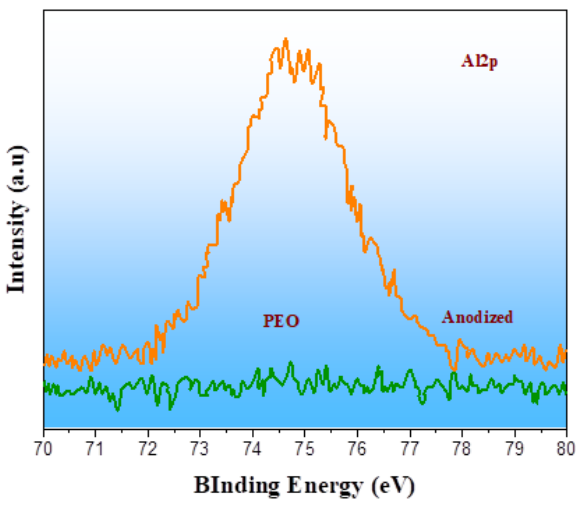

(a)

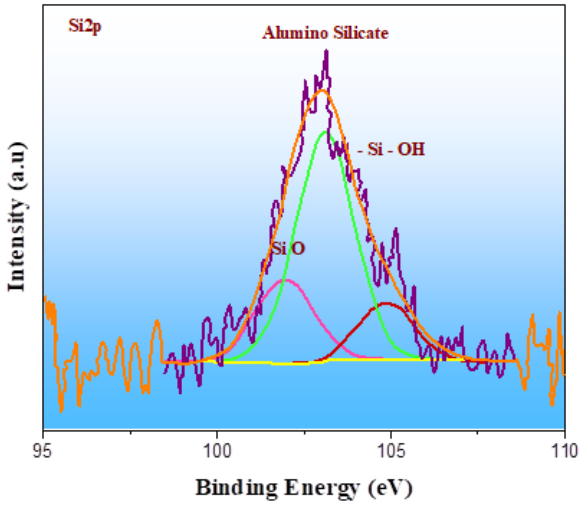

(b)

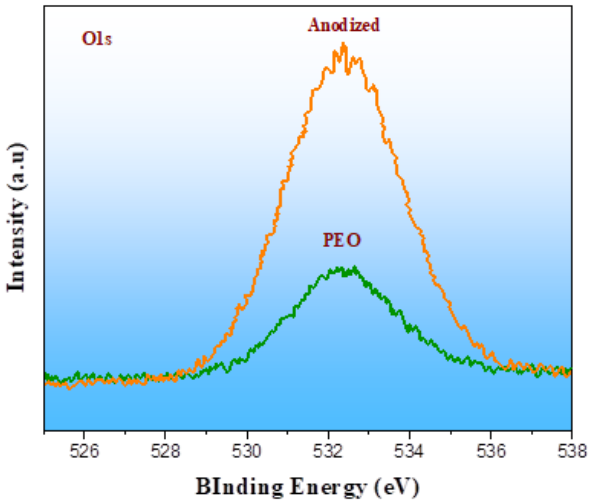

(c)

Fig. 14. (a) The PEO coating's Si2p core-level spectrum, fit to a curve, (b) Anodized and PEO coating O1 score-level spectrum, and (c) Anodized and PEO coatings' Al2p core-level spectrum

3.4 Space Criterion of The Optimum Plasma Electrolytic Oxidation Coating

3.4.1 Photographic Review

The Plasma Electrolytic Oxidation -coated samples are inspected for discontinuities like fractures, patches, excessive buildup, or loose films using a stereo microscope at a magnification of 15. Space simulation tests did not cause any visible damage, color change, or coating deterioration, as seen under a microscope after the samples were put through the ordeal.

3.4.2 Adhesive Testing

The tape peel adhesion test is performed before and after being exposed to the elements. To conduct the test, masking tape is applied over the coated surface. After the tape has been appropriately positioned on the coated outward, a 2-kg rubber-enclosed roller is rolled over it two times. Finally, in one fast action, the tape is taken off. There does not appear to have been any film removal that would expose the substrate surface.

3.4.3 Moisture Test

This procedure replicates the wet, corrosive conditions present just before liftoff to evaluate how well the coating holds up. Authors can learn much about the coating's corrosion resistance and stability under humid storage circumstances by subjecting it to humidity tests at slightly increased temperatures. This procedure is carried out in a humidity chamber with a thermostatically controlled temperature of 52 ± 2°C. The samples are left in a humid environment (96 ± 0.3%) for 48 hours. The coating's integrity is checked visually after each testing round to ensure it hasn't eroded. There was also no discernible shift in the tested values of thermo-optical characteristics.

3.4.4 Thermo-Cycling Test

A spacecraft will experience both extremely cold and scorching temperatures throughout its lifetime. To find out how well a coating can hold up against repeated high and low temperatures, a thermo-cycling test is done. Temperatures in the hot and cold chamber are controlled by a thermostat, ranging from -70°C to +125°C for the test. There are a total of 1500 cycles applied, each lasting 5 minutes at each extreme temperature. The samples' thermo-optical properties did not significantly alter during the thermal cycling test, and a visual check confirmed no damage to the coating afterward.

3.4.5 Thermo-Vacuum Behavior Test

To study the effects of temperature cycling in the harsh space vacuum, a thermo-vacuum performance test is carried out. The process is carried out in a Thermovac chamber at a vacuum of 105 Torr to replicate conditions in space. The PEO-coated samples are cycled through temperatures of +125°C and -70°C for 2 hours at each temperature. This procedure of alternating heat and cold soaks is repeated ten times. The optical properties of the test specimens are then assessed and analyzed after the tests have been completed.

3.4.6 Evaluation of Thermal, Optical Characteristics

After undergoing extensive accelerated aging experiments in a replicated space environment, PEO coatings maintained a consistent thermo-optical behavior. Table 3 shows that the tested values for solar absorption (αS) and infrared Emittance (ƐIR) do not deviate significantly from the as-prepared state.

Recent advancements in PEO-based thermal control coatings have demonstrated that processing parameters and electrolyte design significantly influence solar absorbance (α) and infrared emissivity (ε) on lightweight alloys. For instance, Tu *et al*. reported that PEO coatings on 6061 Al alloy with K_2ZrF_6 additive achieved substantially reduced solar absorbance and enhanced emissivity, with the lowest α (~0.16) and highest ε (~0.72) observed at 15 $g{\cdot}L^{-1}$ additive concentration, attributed to tailored coating thickness and microstructure effects [46]. Other recent studies have explored modified PEO strategies, such as nanoparticle addition to fabricate flat absorber coatings with tailored electric shielding and thermal control on 6061 Al, highlighting multifunctional performance improvements [47]. In contrast to these reports, the current study

systematically optimizes Na_2SiO_3 concentration and electrical parameters specifically for AA5052, achieving a balanced combination of high emissivity and competitive solar absorbance while validating the coating's stability under space-simulated environmental conditions, thus addressing a recognized need for alloy-specific process refinement and durability assessment in thermal control applications.

Table 3. Experimental results of absorptance (αS) and emittance (εIR) before and after testing

S. no.	Experimental Testing	Testing of Solar Absorptance (αS)		Testing of Infrared Emittance (εIR)	
		Before	After	Before	After
1	As received	0.382, 0.371	not applicable	0.96, 0.96	not applicable
2		0.373, 0.382	not applicable	0.98, 0.98	not applicable
3		0.379, 0.377	not applicable	0.98, 0.98	not applicable
4		0.370, 0.371	not applicable	0.98, 0.98	not applicable
5	Moisture	0.386, 0.382	0.393, 0.391	0.96, 0.98	0.98, 0.98
6		0.370, 0.371	0.382, 0.381	0.96, 0.96	0.98, 0.98
7		0.369, 0.371	0.381,0.382	0.83, 0.83	0.98, 0.98
8		0.369, 0.371	0.382, 0.385	0.96, 0.96	0.98, 0.98
9	Thermo-cycling	0.374, 0.372	0.388, 0.386	0.98, 0.98	0.96, 0.96
10		0.376, 0.378	0.395, 0.392	0.96, 0.96	0.96, 0.96
11		0.374, 0.372	0.381, 0.379	0.96, 0.96	0.96, 0.96
12		0.373, 0.370	0.379, 0.388	0.96, 0.96	0.98, 0.96
13	Thermo-vacuum cycling	0.373, 0.371	0.377, 0.373	0.96, 0.96	0.98, 0.98
14		0.373, 0.369	0.378, 0.377	0.96, 0.96	0.98, 0.98
15		0.372, 0.382	0.375, 0.377	0.96, 0.96	0.98, 0.98
16		0.376, 0.382	0.379, 0.378	0.96, 0.96	0.98, 0.98

4. Conclusions

Using a sodium silicate electrolyte and a unipolar pulsed DC square wave current, PEO coatings on AA5052 alloy can be produced. Different operational parameters' effects on the coating's thermo-optical characteristics are studied in depth. This procedure is improved such that Plasma Electrolytic Oxidation coatings with thermal, optical characteristics similar to standard anodic coating can be obtained.

- 1. With a mean coating viscosity of 42 μm and absorption and infra-red emittance values of 0.382 and 0.98, PEO coatings are shown to have a thermal-optical behavior similar to that of standard anodized coating.
- 2. Coatings made under ideal conditions are put through their paces in space by enduring a battery of accelerated aging tests in a laboratory replicating the conditions of outer space. After testing, there was no discernible shift in the coating's thermo-optical properties, including its solar absorption (αS) and infrared Emittance (ƐIR).
- 3. Additional techniques for characterizing the coating include SEM, EDX, XRD, and XPS, with results compared to conventional anodic coating about morphology, microstructure, and composition.

References

[1] Arwati IGA, et al. The influence of temperature and electroforesis deposition green inhibitor on bipolar plate AA5052 in sulfuric acid medium. Sains Malaysiana. 2020;49(12):3169-3177. https://doi.org/10.17576/jsm-2020-4912-28

[2] Pillai AM, Rajendra A, Sharma AK, Sampath S. Development of a solar reflector coating on AA6061 alloy by plasma electrolytic oxidation. J Appl Electrochem. 2019;49(12):1239-1254. https://doi.org/10.1007/s10800-019-01362-7

[3] Nagarajan BM, Manoharan M. Influence of cooling conditions on tensile lap shear strength and microstructure of friction stir welded aluminum alloy 5052-H32 and polycarbonate light weight hybrid joint. J Manuf Process. 2022;82:390-402. https://doi.org/10.1016/j.jmapro.2022.08.008

[4] Liu J, Huang X, Ren Y, Wong LM, Liu H, Wang S. Galvanic corrosion protection of Al-alloy in contact with carbon fibre reinforced polymer through plasma electrolytic oxidation treatment. Sci Rep. 2022;12(1). https://doi.org/10.1038/s41598-022-08727-7
[5] Vasilyeva MS, Lukiyanchuk IV, Yarovaya TP, Rybalka AA. Plasma Electrolytic Synthesis and Study of TiO2-WO3-ZnWO4 Film Heterostructures. Russ J Inorg Chem. 2022;67(9):1451-1459. https://doi.org/10.1134/S0036023622090170
[6] Casanova L, Gruarin M, Pedeferri M, Ormellese M. A study on the debonding of PEO oxides immersed in sulphuric acid through electrochemical impedance spectroscopy. Metall Ital. 2021;113(10):52-57.
[7] Lee JH, Lee YK, Kim YJ, Oh HJ. Surface Characteristics and Photocatalytic Propertiy of B Doped TiO2 Layer Synthesized by Plasma Electrolytic Oxidation Process. Korean J Mater Res. 2021;31(10):552-561. https://doi.org/10.3740/MRSK.2021.31.10.552
[8] Casanova L, Vicentini L, Pedeferri M, Ormellese M. Unipolar plasma electrolytic oxidation: Waveform optimisation for corrosion resistance of commercially pure titanium. Mater Corros. 2021;72(6):1091-1104. https://doi.org/10.1002/maco.202012198
[9] Casanova L, La Padula M, Pedeferri M, Diamanti MV, Ormellese M. An insight into the evolution of corrosion resistant coatings on titanium during bipolar plasma electrolytic oxidation in sulfuric acid. Electrochim Acta. 2021;379. https://doi.org/10.1016/j.electacta.2021.138190
[10] Chizhevskaya MV, Mironova VA, Girn AV, Khodenkova EV. Chemical processes in peo coatings formation and destruction on titanium alloy vt−1. Key Eng Mater. 2021;887:332-338. https://doi.org/10.4028/www.scientific.net/KEM.887.332
[11] Franz S, et al. Exploiting direct current plasma electrolytic oxidation to boost photoelectrocatalysis. Catalysts. 2020;10(3). https://doi.org/10.3390/catal10030325
[12] Engelkamp B, Fischer B, Schierbaum K. Plasma electrolytic oxidation of titanium in H2SO4-H3PO4 Mixtures. Coatings. 2020;10(2). https://doi.org/10.3390/coatings10020116
[13] Aliasghari S, Skeldon P, Zhou X, Hashimoto T. Effect of an anodizing pre-treatment on AA 5052 alloy/polypropylene joining by friction stir spot welding. Mater Sci Eng B Solid-State Mater Adv Technol. 2019;245:107-112. https://doi.org/10.1016/j.mseb.2019.05.018
[14] Serdechnova M, et al. The influence of PSA Pre-Anodization of AA2024 on PEO coating formation: Composition, microstructure, corrosion, and wear behaviors. Materials (Basel). 2018;11(12). https://doi.org/10.3390/ma11122428
[15] Traid HD, Dwojak AN, Vera ML, Ares AE, Litter MI. Porous titanium dioxide coatings synthesized by anodic oxidation. Rev Mater. 2018;23(2). https://doi.org/10.1590/s1517-707620180002.0396
[16] Fakhr Nabavi H, Aliofkhazraei M, Sabour Rouhaghdam A. Morphology and corrosion resistance of hybrid plasma electrolytic oxidation on CP-Ti. Surf Coatings Technol. 2017;322:59-69. https://doi.org/10.1016/j.surfcoat.2017.05.035
[17] Yan Z, Wu M, Qin H, He Y, Yu X, Chen L. ZrO2/TiO2 films prepared by plasma electrolytic oxidation and a post treatment. Surf Coatings Technol. 2017;309:331-336. https://doi.org/10.1016/j.surfcoat.2016.11.086
[18] Hong SM, Tashiro S, Bang HS, Tanaka M. Numerical analysis on thermal characteristics of direct current pulsed gas metal arc welded joints of AA5052 aluminum alloy to DP590 high strength steel. Quarterly J Japan Weld Soc. 2021;38(2):93S-97S. https://doi.org/10.2207/qjjws.38.93s
[19] Aubakirova V, Farrakhov R, Astanin V, Parfenov E, Sharipov A, Gorbatkov M. Plasma Electrolytic Oxidation of Zr-1%Nb Alloy: Effect of Sodium Silicate and Boric Acid Addition to Calcium Acetate-Based Electrolyte. Materials (Basel). 2022;15(6). https://doi.org/10.3390/ma15062003
[20] Premchand C, et al. Assessment of Corrosion and Scratch Resistance of Plasma Electrolytic Oxidation and Hard Anodized Coatings Fabricated on AA7075-T6. Trans Indian Inst Met. 2021;74(8):1991-2002. https://doi.org/10.1007/s12666-021-02289-4
[21] Zhu L, Ke X, Li J, Zhang Y, Zhang Z, Sui M. Growth mechanisms for initial stages of plasma electrolytic oxidation coating on Al. Surfaces and Interfaces. 2021;25. https://doi.org/10.1016/j.surfin.2021.101186
[22] Madhuri D, et al. Development and Characterization of High Emittance and Low-Thickness Plasma Electrolytic Oxidation Coating on Ti6Al4V for Spacecraft Application. J Mater Eng Perform. 2021;30(6):4072-4082. https://doi.org/10.1007/s11665-021-05862-6
[23] Pillai AM, et al. Crystalline and amorphous PEO based ceramic coatings on AA6061: Nanoindentation and corrosion studies. Ceram Int. 2021;47(10):14707-14716. https://doi.org/10.1016/j.ceramint.2021.01.147
[24] Husak Y, et al. Bioactivity performance of pure mg after plasma electrolytic oxidation in silicate-based solutions. Molecules. 2021;26(7). https://doi.org/10.3390/molecules26072094
[25] Baghdadabad DM, Baghdadabad ARM, Khoei SMM. Characterization of bioactive ceramic coatings synthesized by plasma electrolyte oxidation on AZ31 magnesium alloy having different Na2SiO3·9H2O concentrations. Mater Today Commun. 2020;25. https://doi.org/10.1016/j.mtcomm.2020.101642

[26] Asare-Addo K, Totea AM, Nokhodchi A. Drug release from magnesium aluminium silicate-polyethylene oxide (PEO) nanocomposite matrices: An investigation using the USP III apparatus. Eur J Pharm Sci. 2020;153. https://doi.org/10.1016/j.ejps.2020.105474
[27] Klobčar D, et al. Influence of Friction Riveting Parameters on the Dissimilar Joint Formation and Strength. Materials. 2022;15(19). https://doi.org/10.3390/ma15196812
[28] Sharma V, Mallick A, Kumar K. Effect of graphene nanoplates on the mechanical and corrosion properties of aluminium nanocomposite fabricated by powder metallurgy. Tribol Mater. 2023;2(4):154-161. https://doi.org/10.46793/tribomat.2023.018
[29] Vencl A, Rac A, Bobić I, Mišković Z. Tribological properties of Al-Si alloy A356 reinforced with Al2O3 particles. Tribology in Industry. 2006;28(1-2):27-31.
[30] Kumar P, Srivastava VK, Sharma A. Influence of cooling mediums on mechanical and tribological characteristics of Al/Cu-based composites reinforced with chromium particles. Tribology and Materials. 2025;4(3):134-143. https://doi.org/10.46793/tribomat.2025.016
[31] Pezzato L, Settimi AG, Cerchier P, Gennari C, Dabalà M, Brunelli K. Microstructural and corrosion properties of PEO coated zinc-aluminized (ZA) steel. Coatings. 2020;10(5). https://doi.org/10.3390/coatings10050448
[32] Ramadani AIWS, et al. Ordered structure analysis of prepared mesoporous silica using small angle X-Ray scattering. Atom Indones. 2020;46(1):11-17. https://doi.org/10.17146/aij.2020.835
[33] Yao Z, et al. Preparation of black high absorbance and high emissivity thermal control coating on Ti alloy by plasma electrolytic oxidation. Surf Coatings Technol. 2014;253:166-170. https://doi.org/10.1016/j.surfcoat.2014.05.032
[34] Yao Z, Shen Q, Niu A, Hu B, Jiang Z. Preparation of high emissivity and low absorbance thermal control coatings on Ti alloys by plasma electrolytic oxidation. Surf Coatings Technol. 2014;242:146-151. https://doi.org/10.1016/j.surfcoat.2014.01.034
[35] Sevidova E, Pupan L, Gutsalenko Y, Rudnev A, Titarenko O. Effect of Morphological Features on Dielectric Properties of Plasma Electrolytic Oxidation Coatings on D16T Aluminum Alloy. In: Lecture Notes in Mechanical Engineering. 2020. p. 542-551. https://doi.org/10.1007/978-3-030-50794-7_53
[36] Sevidova E, Gutsalenko Y, Rudnev A, L. Pupan, Titarenko O. The study of surface microgeometry and morphology of plasma electrolytic oxidation dielectric coatings on aluminum alloys. In: Lecture Notes in Mechanical Engineering. 2020. p. 302-310. https://doi.org/10.1007/978-3-030-22365-6_30
[37] Aliasghari S, Skeldon P, Zhou X, Hashimoto T. Effect of electrolyte composition on morphology and corrosion resistance of plasma electrolytic oxidation coatings on aluminized steel. Surf Coatings Technol. 2019;372:239-251. https://doi.org/10.1016/j.surfcoat.2019.05.047
[38] Xia Q, Zhang D, Li D, Jiang Z, Yao Z. Preparation of the plasma electrolytic oxidation coating on Mg-Li alloy and its thermal control performance. Surf Coatings Technol. 2019;369:252-256. https://doi.org/10.1016/j.surfcoat.2019.04.073
[39] Molaei M, Fattah-Alhosseini A, Keshavarz MK. Influence of different sodium-based additives on corrosion resistance of PEO coatings on pure Ti. J Asian Ceram Soc. 2019;7(2):247-255. https://doi.org/10.1080/21870764.2019.1604609
[40] Pezzato L, Cerchier P, Brunelli K, Bartolozzi A, Bertani R, Dabalà M. Plasma electrolytic oxidation coatings with fungicidal properties. Surf Eng. 2019;35(4):325-333. https://doi.org/10.1080/02670844.2018.1441659
[41] Tavares MDM, et al. Effect of duty cycle and treatment time on electrolytic plasma oxidation of commercially pure Al samples. J Mater Res Technol. 2019;8(2):2141-2147. https://doi.org/10.1016/j.jmrt.2019.01.020
[42] Xi Z, Zhou S, Jin L. Experimental investigation of self-hardening foam-sol for controlling diffusion of static coal dust. Powder Technol. 2019;345:274-282. https://doi.org/10.1016/j.powtec.2019.01.023
[43] Wu Y, et al. Effects of one-step and two-step treatment regimes on the characteristics of Plasma Electrolytic Oxidation (PEO) coatings on aluminum. Int J Electrochem Sci. 2019;14(5):4730-4753. https://doi.org/10.20964/2019.05.19
[44] Ramakrishnan E, Premchand C, Manojkumar P, Rameshbabu N. Development of thermal control coatings on AA7075 by plasma electrolytic oxidation (PEO) process. Mater Today Proc. 2021;46:1085-1090. https://doi.org/10.1016/j.matpr.2021.01.436
[45] Zhang K, et al. A self-curing konjac glucomannan/CaCO3 coating for corrosion protection of AA5052 aluminum alloy in NaCl solution. Int J Biol Macromol. 2020;151:691-701. https://doi.org/10.1016/j.ijbiomac.2020.02.223
[46] Tu C, Chen X, Liu C, Li D. Plasma Electrolytic Oxidation Coatings of a 6061 Al Alloy in an Electrolyte with the Addition of K2ZrF6. Materials. 2023;16(11). https://doi.org/10.3390/ma16114142
[47] Ji R, et al. A controllable fabrication of flat absorber dual-layer coating with electric shielding on 6061 aluminum alloy by PEO with nanoparticles additive. Surf Coatings Technol. 2023;459:129382. https://doi.org/10.1016/j.surfcoat.2023.129382